

FLOW FIELD INTERFERENCE CHARACTERISTIC OF AXIAL RING WING CONFIGURATION

Q. Duo^{1*} – F. Jinfu¹ – Z. Jiaqiang² – L. Yongli³

¹Aeronautics and Astronautics Engineering College, Air Force Engineering University, Xi'an 710038, China

²Air Traffic Control and Navigation College, Air Force Engineering University, Xi'an 710051, China

³Engineering University of CAPF, Xi'an 710086, China

ARTICLE INFO

Article history:

Received: 25.10.2014.

Received in revised form: 19.03.2014.

Accepted: 20.03.2014.

Keywords:

Axial ring wing

Aerodynamic configuration

Numerical simulation

Interference characteristic

SST $k-\omega$ turbulence model

Abstract:

To analyze the air flow interference between upper and lower wings in axial ring wing configuration, NASA SC(2)-1006 supercritical airfoil is chosen as the basic airfoil. Flow field around the double-wing structure with different relative distances between upper and lower wings is numerically simulated, using SST $k-\omega$ turbulence model, and the numerical conclusion about the influence of relative distance D/L on the aerodynamic performance is drawn. It is shown that, at the speed $Ma = 0.8$, reflection of shockwave between the upper wing and the lower wing has a great negative effect on both lift and drag coefficient. When $D/L = 0.1$, and the angle of attack $AOA = 0^\circ$, the resultant lift produced by the two wings is equivalent to that of the single wing, while the resultant drag is 4 times of that of the single wing, which shows a poor aerodynamic characteristic. With the increasing of the relative distance, the intensity of the shockwave between the upper and lower wings is weakened and the negative effect is relieved. Furthermore, the growth of the angle of attack AOA can obscure the negative effect. It could provide helpful reference to the design of axial ring wing aircraft.

1 Introduction

As a form of nonplanar wing, the ring wing, by right of its special configuration, expresses many advantages such as light weight and good maneuverability. On the same lift condition, the span of a ring wing is smaller and it has better resistance to bending and flexing when compared with the planar wing by configuration parameter optimization [1, 2]. Many people have researched

the application of ring wing in transport aircraft, unmanned aerial vehicles, missiles, torpedoes and other platforms for a long time. IR & D project, led by Hughes, studied the stretchable ring wing (Extendable Ring Wing) to increase the range, payload and terminal mobility of weapons and underwater unmanned aircraft. It has conducted experimental research in the AEDC 1.22 m transonic wind tunnel [3, 4]. However, conducting experiments in a wind tunnel or water tunnel will be

* Corresponding author. Tel: +86 029 84787514; fax: +86 029 84787514
E-mail address: qj33song@sina.com

time-consuming and expensive, and it is hard to change the boundary conditions. CFD simulation has some advantages such as being quick, economical, intuitive, and easy to conduct [5]. It also has incomparable superiority in displaying and analyzing the pressure and velocity distribution of the flow field.

Ring wing has two forms: radial and axial. With aircraft airfoil chord line perpendicular to the aircraft axis, the radial ring wing is mainly applied to new concept aircrafts, such as unmanned aerial vehicles. With airfoil axial chord line parallel to the aircraft axis, the axial ring wing is applied to space constrained weapons which are wrapped by ring wings when stored, and can greatly reduce the occupied space; after launch, the ring wing lifting surface can increase the range of weapons.

When air flows through the ring wing, the flow will be disturbed by the hollow cavity between the wings, and changes dramatically. The interaction between airflow and structure of the upper and lower wings is more complex than monoplane structure [6]. Studying its mechanism is important to parameters optimization of ring wing.

2 Physical model

A typical layout of axial ring wing in references [3] is shown in Fig. 1.

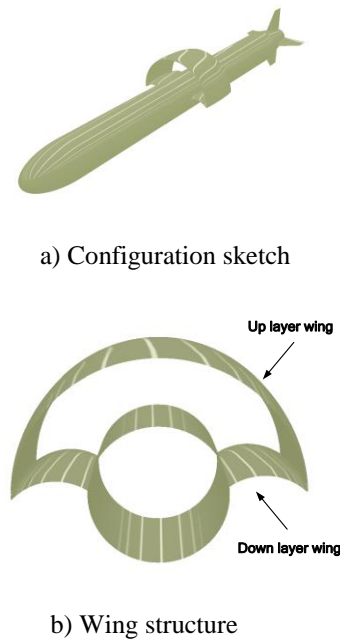


Figure 1. An axial ring wing configuration.

In this paper, NASA SC(2)-1006 supercritical airfoil [7] is chosen as the longitudinal section of ring wing to study the aerodynamic characteristics and flow field of the upper and lower wings, and to analyze the aerodynamic parameters change with respect to the dimensionless parameter D/L (where, D is the space distance between the two wings, L is the chord length). The layout of the longitudinal section is shown in Fig. 2.

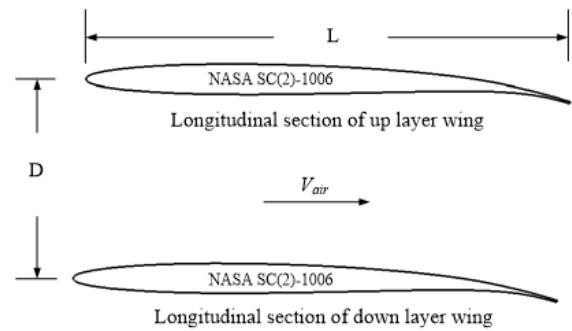


Figure 2. Longitudinal section of axial ring wing configuration.

3 Turbulence model

The SST $k-\omega$ turbulence model is used in numerical simulation, which is developed by Menter and has been proved highly accurate and reliable in a wide range of flow fields [8, 9]. Its core idea is to use the $k-\omega$ model in the near wall region, $k-\varepsilon$ model in the free shear layer (add cross-diffusion term), and to combine the two models by a hybrid function F_1 to achieve the transition from the $k-\omega$ model to the $k-\varepsilon$ model. The concrete form is shown in reference [10].

To meet the intense pressure gradient change near the wall, hybrid function F_2 is introduced into the SST model to amend the turbulent viscosity coefficient:

$$v_t = \frac{a_1 k}{\max(a_1 \omega, \Omega F_2)}, \quad (1)$$

$$F_2 = \tanh(\arg_2^2), \quad (2)$$

$$\arg_2 = \max \left[2 \frac{\sqrt{k}}{0.09 \omega y}, \frac{500 \nu}{y^2 \omega} \right], \quad (3)$$

In the formula, shear strain rate is $\Omega = |\partial u / \partial y|$. In SST $k-\omega$ model, the parameters collection ϕ including σ_{kl} , $\sigma_{\omega 1}$, β , β^* , γ is combined by two groups of parameters, namely:

$$\phi = F_1 \phi_1 + (1 - F_1) \phi_2. \quad (4)$$

In the formula, the inner parameter ϕ_1 corresponding to the Wilcox $k-\omega$ model, is shown as follows:

$$a_1 = 0.31, \sigma_{kl} = 0.85, \sigma_{\omega 1} = 0.5, \beta_1 = 0.075,$$

$$\beta^* = 0.09, \kappa = 0.41, \gamma_1 = \beta_1 / \beta^* - \sigma_{\omega 1} \kappa^2 / \sqrt{\beta^*}.$$

The outer parameter ϕ_2 , corresponding to the standard $k-\varepsilon$ model, is shown as follows:

$$a_1 = 0.31, \sigma_{k2} = 1.0, \sigma_{\omega 2} = 0.856, \beta_1 = 0.0828,$$

$$\beta^* = 0.09, \kappa = 0.41, \gamma_2 = \beta_2 / \beta^* - \sigma_{\omega 2} \kappa^2 / \sqrt{\beta^*}.$$

4 Computational model and boundary conditions

The structure parameters of NASA SC(2)-1006 supercritical airfoil are shown in Table 1.



Figure 3. Structure of NASA SC(2)-1006 Supercritical Airfoil.

Table 1. NASA SC(2)-1006 supercritical airfoil structure parameters

x/L	(y/L) _u	(y/L) _l	x/L	(y/L) _u	(y/L) _l
0.000	0.000	0.000	0.600	0.0198	-0.026
0.100	0.230	-0.226	0.700	0.0117	-0.024
0.200	0.0285	-0.028	0.800	0.0001	-0.023
0.300	0.300	-0.030	0.900	-0.0184	-0.028
0.400	0.0288	-0.029	1.000	-0.0443	-0.048
0.500	0.0254	-0.028	-	-	-

For the double-wing structure features of axial ring wing, the computational domain is divided into double O-type structure grids, as shown in Fig. 4.

Regional grids, where shockwave may occur, are locally encrypted. The flow velocity is 0.8 Ma, and second-order upwind difference scheme is selected to discretize N-S equations. To make $y^+ < 1$, the thickness of the first layer of mesh is 3×10^{-6} times of the chord length. The far field is 20 times as long as the chord length, and the number of meshes is about 60 thousand, $Re = 1.117 \times 10^7$.

The boundary conditions for the simulation are as follows: The undisturbed uniform velocity is given at the domain inlet, and the averaged static pressure is set at the domain outlet. The outer wall of the domain is regarded as the free slip wall while the solid surface of the airfoil is set as the nonslip wall. For the velocity and pressure coupling, the SIMPLEC algorithm is used.

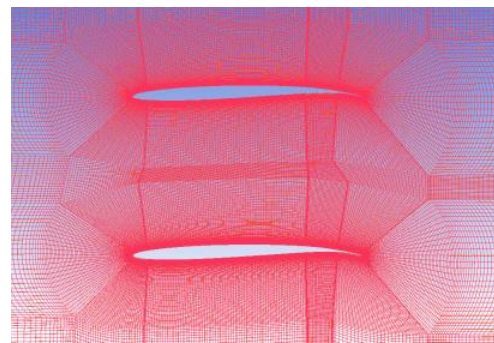


Figure 4. Partial double O Grid (D/L = 0.7).

5 Aerodynamic characteristics analysis

Five configurations' aerodynamic characteristics of the relative distance between the upper and lower wings $D/L = 0.1, 0.4, 0.7, 1.0$ and single-wing structure are simulated, the angle of attack (AOA) being 0, 3, 6 and 9°, respectively. Considering the huge number of meshes in 3D flow field and it has a higher requirements for the simulation environment, 2D flow field is adopted in this study.

The normal flight of an aircraft is always under small AOA conditions and $AOA = 3^\circ$ is representative. The simulation results show that, pressure and velocity distribution characteristics on other AOA conditions are similar with that of $AOA = 3^\circ$. The pressure (Pa), velocity (Ma), contour plots at $AOA = 3^\circ$ are shown in Fig. 5 [a-j].

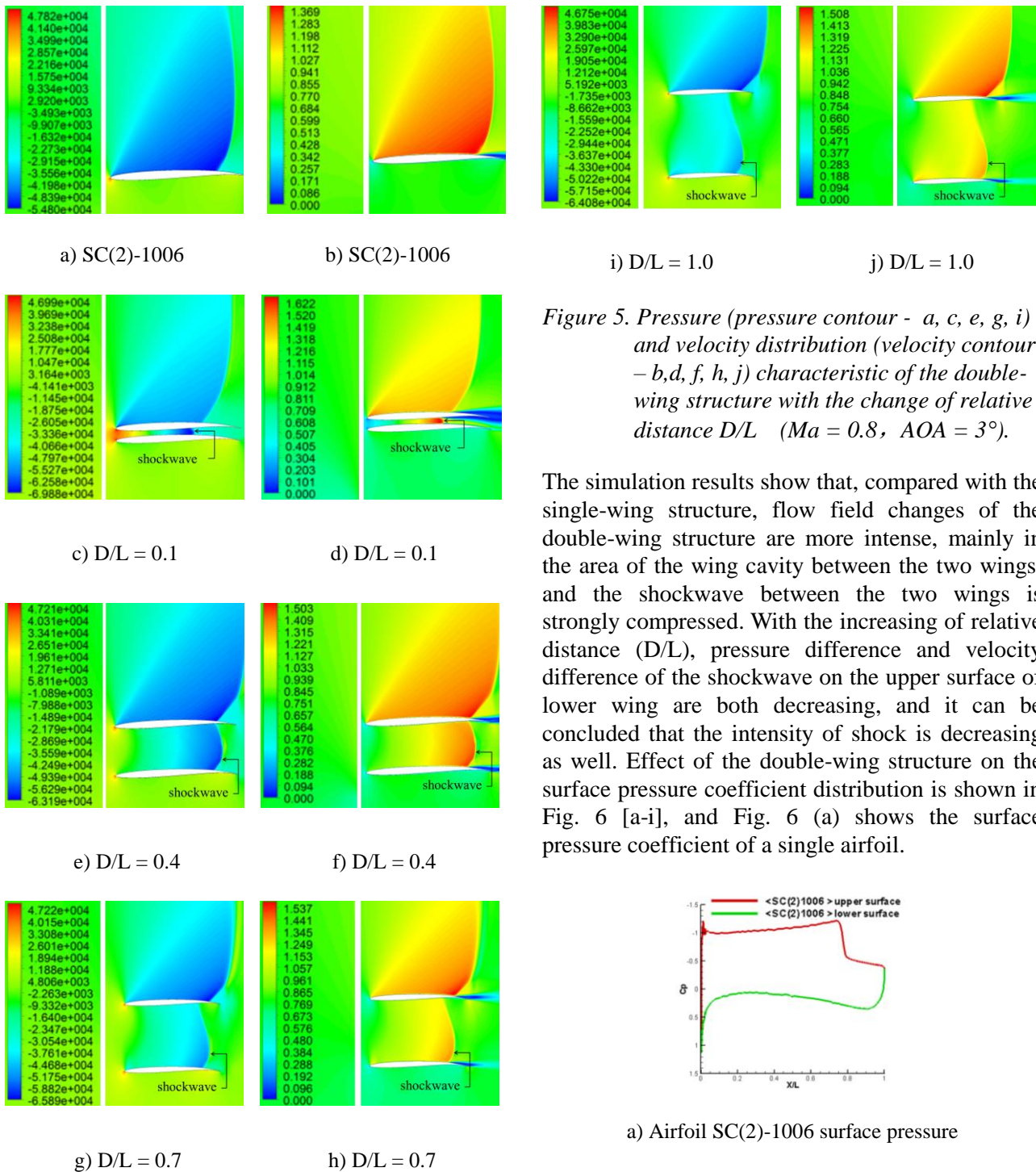
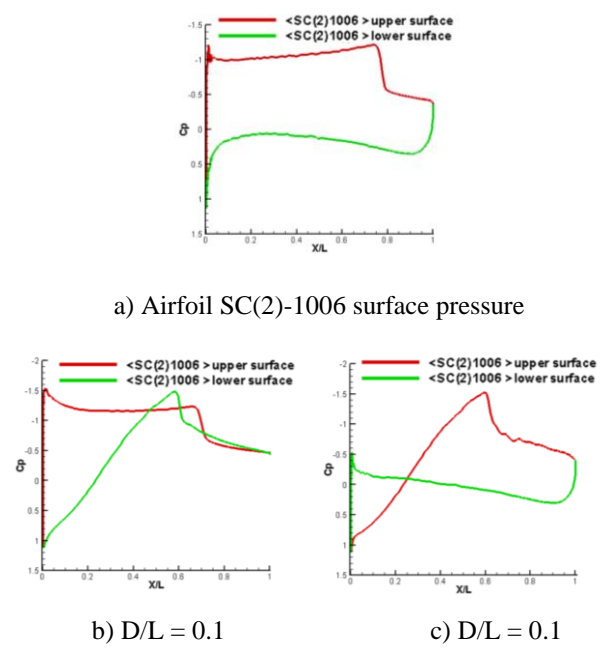


Figure 5. Pressure (pressure contour - a, c, e, g, i) and velocity distribution (velocity contour - b, d, f, h, j) characteristic of the double-wing structure with the change of relative distance D/L ($Ma = 0.8$, $AOA = 3^\circ$).

The simulation results show that, compared with the single-wing structure, flow field changes of the double-wing structure are more intense, mainly in the area of the wing cavity between the two wings, and the shockwave between the two wings is strongly compressed. With the increasing of relative distance (D/L), pressure difference and velocity difference of the shockwave on the upper surface of lower wing are both decreasing, and it can be concluded that the intensity of shock is decreasing as well. Effect of the double-wing structure on the surface pressure coefficient distribution is shown in Fig. 6 [a-i], and Fig. 6 (a) shows the surface pressure coefficient of a single airfoil.



a) Airfoil SC(2)-1006 surface pressure

b) $D/L = 0.1$

c) $D/L = 0.1$

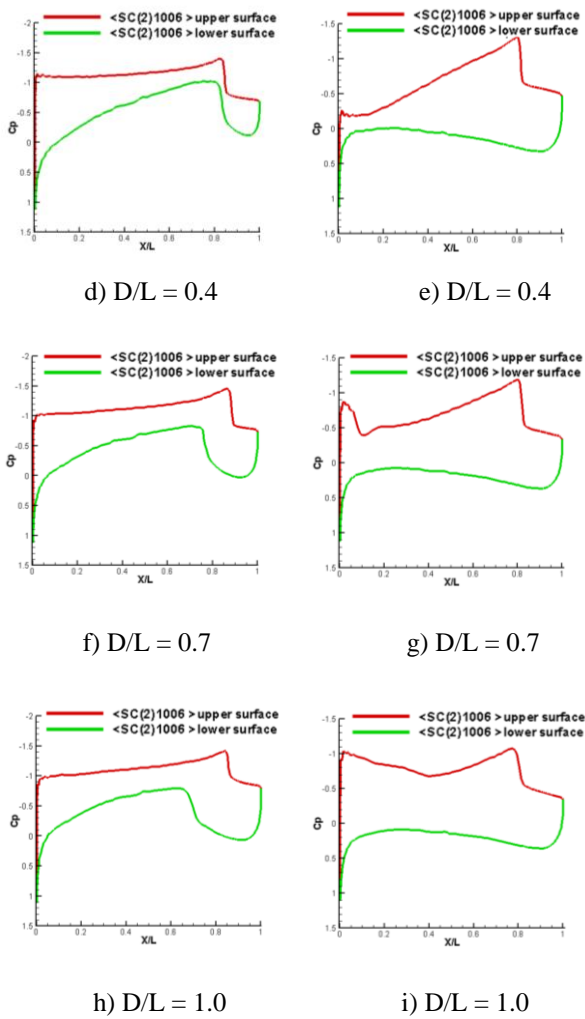


Figure 6. Surface pressure distribution characteristic (upper wing pressure – b, d, f, h, and lower wing pressure – c, e, g, i) of the double airfoil structure ($Ma = 0.8$, $AOA = 3^\circ$).

Fig. 6 shows the presence of strong aerodynamic interference between the upper and lower wings of double-wing structure. Compared with the pressure distribution on the upper and lower surfaces of single-wing structure, significant changes take place on the lower surface of upper wing and the upper surface of lower wing of double-wing structure. For the upper wing, two shockwaves occur on the upper and lower surfaces, and the interference increases rapidly with the relative distance (D/L) reducing. It can be seen from Fig. 5 (b) and 5 (c) that lift reversal phenomenon occurs in the rear of the upper wing and in the front of lower wing when $D/L = 0.1$. The trend of upper and lower wing aerodynamic coefficients with the relative distance changing is

shown in Fig. 7 [a–h], in contrast with a single-wing structure aerodynamic, the upper and lower wings aerodynamic and the overall aerodynamic of double-wing structure are shown in each figure.

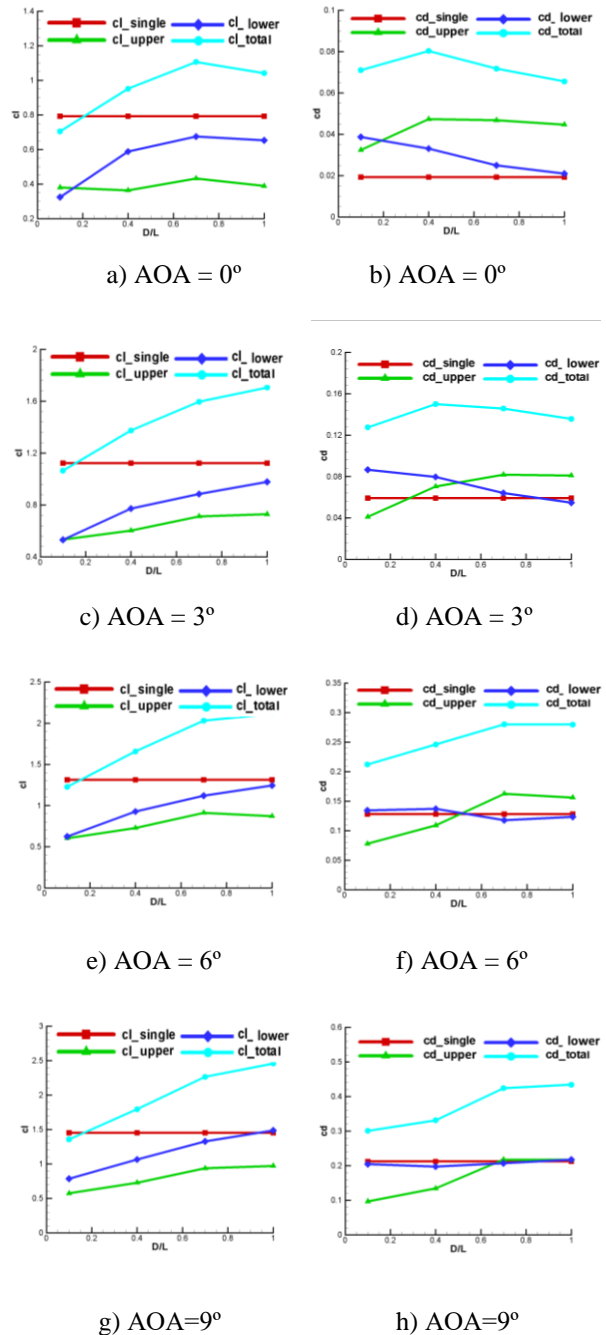
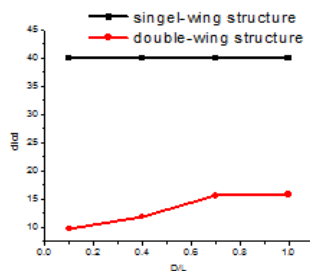


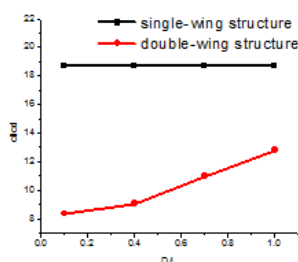
Figure 7. $AOA = 0 \sim 9^\circ$, aerodynamic coefficient (lift coefficient – a, c, e, g, and drag coefficient b, d, f, h) changing tendency of upper and lower wings along with relative distance D/L ($Ma = 0.8$).

In terms of the lift characteristics, the upper wing suffered far greater lift losses than that of the lower wing. On the condition that $AOA = 0^\circ$, when relative distance $D/L = 0.1$, the lift of two wings is only half of the single wing. With the D/L increasing, the lift of lower wing recovers gradually and increases to 80% of the single wing when $D/L = 1.0$, while the lift of the upper wing stay at a low level (about 50% of that of the single wing configuration). On $6^\circ, 9^\circ$ AOA conditions, with D/L increasing from 0.1 to 1.0, the lower wing lift increases from 50% to nearly 100% of the single wing lift; and the upper wing lift is increased from 30 to 70% of the single wing lift.

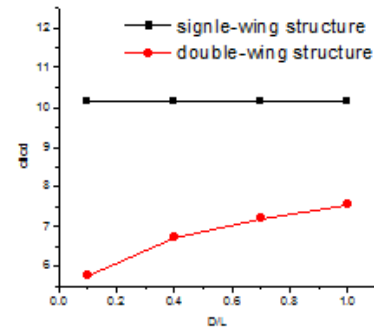
As for the drag characteristics, when $AOA = 0^\circ$, our configuration makes the lower and upper wing drag double ($D/L = 0.1$) that of the single configuration, and the lower wing drag is reduced when increasing the D/L ; when $D/L = 1.0$, the drag reaches the level of a single wing, but the upper wing drag shows a tendency to increase with D/L increasing and tends to be stable when $D/L > 0.4$. As the AOA increases, the lower wing drag constantly approaches the level of the single wing drag, and after the AOA is greater than 6° , the two drag values converge, as shown in Fig. 7 (f) and 7 (h). The tendency that the upper wing drag increases with D/L does not changed with the AOA increasing. But as the AOA increases, when the relative distance is small, for example, $D/L = 0.1$, its drag is smaller than that of the single wing under the same AOA.



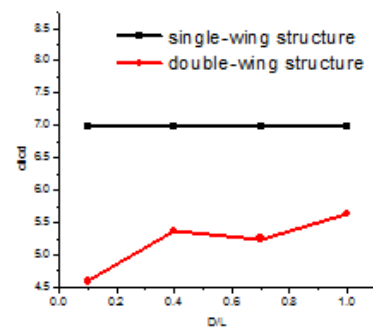
a) AOA = 0° cl/cd ratio



b) AOA=3° cl/cd ratio



c) AOA = 6° cl/cd ratio



d) AOA = 9° cl/cd ratio

Figure 8. AOA = 0 ~ 9°, cl/cd ratio of single-wing structure and double-wing structure.

Fig. 8 shows the lift to drag ratio when $AOA = 0 \sim 9^\circ$. It can be seen that, on the condition of 2D airfoil model, in general, with the AOA increasing, the lift to drag ratios of single-wing structure and double-wing structure are both decreasing. However, the lift to drag ratio of single-wing structure is higher. On the one hand, air flow reflected by the upper wing has a negative effect on the lower wing, which slows down the flow velocity on the lower wing and reduces the lift; on the other hand, drag is increased because of the flow interference on the wingtip.

6 Conclusion

In this paper, NASA SC(2)-1006 supercritical airfoil is chosen as the basic airfoil to study the axial ring wing interference characteristics of the air flow. The flow field between the upper and lower wing is numerically simulated on different conditions of relative distance, and the change rule that how the relative distance D/L influences the upper and lower wings' aerodynamic characteristics

is obtained. The simulation results show that the shockwave on the upper surface of the lower wing has a great negative impact on the upper and lower lift and drag coefficients because of the reflection effect of the upper wing; and with the increasing of the relative distance D/L , the cavity shock strength decreases, so this adverse effect is weakened. Besides, geometrical shapes of the airfoil affect flow field interference characteristic of axial ring wing configuration, and it will be considered in the further study.

References

- [1] Hou, S., Xing Y.: *Ring Wing for Underwater Missile*, Winged Missiles Journal, (2004), 3, pp. 19-21.
- [2] Li, M., Deng, Y.M.: *The Aerodynamics Research of Ring Wing Configuration in Low Speed Wind Tunnel*, Aircraft Design, 28 (2008), 6, pp. 1-5.
- [3] August, H., Osborn, R., Pinney, M.: *Ring Wing Missile for Compressed Carriage on An Aircraft*, AIAA Atmospheric Flight Mechanics Conference, Monterey, CA, Aug. 9-11, 1993.
- [4] August, H., Carapezza, E.: *Ring Wing for an Underwater Missile*, AIAA Atmospheric Flight Mechanics Conference, Monterey, CA, Aug. 9-11, 1993.
- [5] Percic, M., Lenic, K., Trp, A.: *A three-dimensional numerical analysis of complete crossflow heat exchangers with conjugate heat transfer*, Engineering Review, 33 (2013), 1, pp. 23-40.
- [6] Kruggel, B., McLaughlin, E.: *Aerodynamic Characteristics of A Conformal Ring Wing and Wrap around Fin System*, AIAA Applied Aerodynamics Conference, 16th, Albuquerque, NM, June 15-18, 1998, pp.773-777.
- [7] Harris, C.D.: *NASA supercritical airfoils A matrix of family-related airfoils*, Langley Research Center, 1990.
- [8] Wu, X.J., Ma, M.S., Deng, Y.Q.: *Two turbulence models for the computation of transonic flow*, Acta Aerodynamica Sinica, 26(2008),1, pp. 85-90.
- [9] Zhou, Y., Qian, W.Q., Deng, Y.Q.: *Introductory analysis of the influence of Menter's $k-\omega$ SST turbulence model's parameters*, Acta Aerodynamica Sinica, 28 (2010), 2, pp. 213-217.
- [10] Florian, R., Menter.: *Zonal two equation $K-\omega$ turbulence models for aerodynamic flows*, Ames Research Center, 1993.